Tracking C-H activation with orbital resolution

Raphael M. Jay[1,*,†] Ambar Banerjee[1,*,†], Torsten Leitner[1], Ru-Pan Wang[2], Jessica Harich[2], Robert Stefanuik[1], Hampus Wikmark[1], Michael R. Coates[3], Emma V. Beale[4], Victoria Kabanova[4], Abdullah Kahraman[4], Anna Wach[4,5], Dmitry Ozerov[4], Christopher Arrell[4], Philip J. M. Johnson[4], Camelia N. Borca[4], Claudio Cirelli[4], Camila Bacellar[4], Christopher Milne[6], Nils Huse[2], Grigory Smolentsev[4], Thomas Huthwelker[4], Michael Odelius[3], Philippe Wernet[1,*]

[1]Department of Physics and Astronomy, Uppsala University, 751 20 Uppsala, Sweden.

[2]Center for Free-Electron Laser Science, Institute for Nanostructure and Solid State Physics, University of Hamburg, 22761 Hamburg, Germany.

[3]Department of Physics, Stockholm University, 106 91 Stockholm, Sweden.

[4]Paul-Scherrer Institute, CH-5232 Villigen PSI, Switzerland.

[5]Institute of Nuclear Physics, Polish Academy of Sciences, PL-31342 Krakow, Poland.

[6]European XFEL GmbH, 22869 Schenefeld, Germany.

*Corresponding author. Email: raphael.jay@physics.uu.se, ambar.banerjee@physics.uu.se, philippe.wernet@physics.uu.se

[†]The authors contributed equally to this work.

Abstract: The reactivity towards C-H bond activation of alkanes with transition metals is determined by the ability of the metal to donate and withdraw electron density in due proportion. Manipulating this reactivity in a controlled way is difficult, because the hypothesized metal-alkane charge-transfer interactions are challenging to access experimentally. Using time-resolved X-ray spectroscopy, we track the charge-transfer interactions in a C-H activating Rh complex and reveal changes in oxidation state as well as valence-orbital energies and character from femtosecond Rh-alkane bond formation to nanosecond C-H bond cleavage. Our X-ray spectroscopic signatures reflect how alkane-to-metal donation determines metal-alkane bond stability and how metal-to-alkane back-donation facilitates C-H bond cleavage by oxidative addition. The ability to dissect charge-transfer interactions on an orbital-level provides new opportunities for manipulating reactivity for C-H activation with transition metals.

The transformation of saturated hydrocarbons under mild conditions into more valuable products constitutes a long-standing challenge in chemistry (*1–4*). Making methane and higher alkanes readily available as abundant and cheap raw materials for chemical synthesis relies on the ability to selectively and efficiently cleave inert C-H bonds for further functionalization. Ever since their first observation (*5*, *6*), photochemical routes employing transition metal complexes have become established ways for activating C-H bonds in room-temperature solution (*1*, *2*, *4*, *7*). Photo-induced ligand loss from the metal complex is known to create a highly reactive species with an undercoordinated and electron-deficient metal center (exemplary scheme in Fig. 1A for the here-studied complex). The metal then rapidly binds an alkane C-H group from solution and forms a σ-complex, in which the C-H group coordinates with the metal via one of its σ-bonds. Ultimately, by being inserted between C and H in the reaction, the metal breaks the C-H bond to form a metal alkyl hydride product. σ-complexes are the decisive reaction intermediates and have therefore been extensively studied over the past decades in terms of their molecular structure and mechanistic role (*8–18*).

Quantum chemical calculations, in particular, suggest that the metal-alkane bond in σ-complexes is formed by donation of electron density from the occupied C-H σ-orbital into unoccupied metal d-orbitals concomitant to back-donation from occupied metal d-orbitals into the unoccupied antibonding C-H σ^*-orbital (*19–22*) (similar to, albeit significantly weaker than metal-carbonyl bonds as illustrated in Fig. 1B). Both types of interactions at the same time enhance metal-alkane bonding and weaken the alkane C-H bond. Since it is the balance of back-and-forth charge-transfer via different orbitals which determines whether a σ-complex ultimately proceeds to C-H bond cleavage, dissecting individual charge-transfer interactions could provide orbital-based design principles as a guide for catalyst development. Experimentally, time-resolved infrared spectroscopy has been instrumental in identifying reaction intermediates in C-H activation (*15*) by probing shifts in infrared marker modes of spectator ligands. Such shifts are the result of changes in spectator-ligand bond strengths induced by changes of the integrated charge-transfer interactions in the complex. Separately accessing donation and back-donation to and from the metal in a σ-complex, however, would be a way to experimentally correlate individual orbital interactions with reactivity towards C-H bond cleavage (*7*).

Here, we demonstrate a new way to experimentally evaluate metal-ligand charge-transfer interactions in C-H activation with metal complexes. Using time-resolved X-ray absorption spectroscopy (XAS) at the metal L-edge (*23–28*), we select in time the short-lived reaction intermediates and in space the reactive metal site to interrogate the decisive charge-transfer interactions that determine the overall reaction. In two UV-pump and X-ray probe experiments at the Swiss Free Electron Laser facility (SwissFEL) and the Swiss Light Source synchrotron radiation facility (SLS), we track σ-complex formation and oxidative addition using CpRh(CO)$_2$ (where Cp = cyclopentadienyl) (*10*, *16–18*) in octane solution. The time-resolved Rh L-edge absorption spectra were recorded by collecting the X-ray fluorescence as a function of incident X-ray photon energy around the Rh L$_3$ absorption edge (Fig. 1C and Supporting information for experimental details). As in the case of other 4d transition metal complexes (*25*, *29*, *30*), the Rh L$_3$-edge transitions can be assigned to excitations of Rh 2p core electrons to unoccupied molecular orbitals (see Fig. 1D). Changes in transition energies reflect changes in orbital energies, whereas oscillator strengths vary with the degree to which Rh 4d and ligand orbitals hybridize (see Supporting Information). In combination with our calculations, this provides direct access to back-and-forth charge-transfer interactions along the C-H activation reaction down to the level of individual orbitals.

The steady-state Rh L$_3$-edge absorption spectrum of CpRh(CO)$_2$ shown in Fig. 1D exhibits a peak at a photon energy of ~3006 eV that results from excitation of Rh 2p core-electrons into
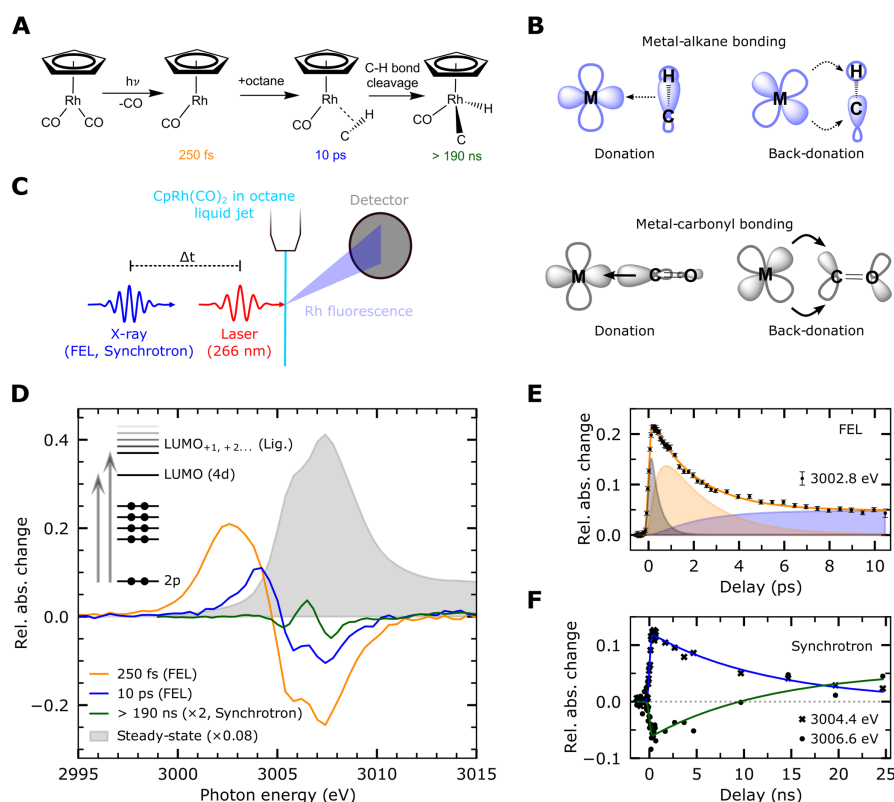
Fig. 1. Basic mechanisms and time-resolved X-ray absorption spectroscopy of C-H activation with CpRh(CO)₂ in octane solution. (**A**) Schematic of C-H activation by CpRh(CO)₂ via photo-induced oxidative addition. (**B**) Orbital-specific metal-ligand charge-transfer interactions for metal-carbonyl and metal-alkane bonds. (**C**) Schematic of the experiment with UV laser pump pulses triggering the reaction and X-ray pulses probing orbital evolution as a function of time delay between pump and probe pulses. Photo-induced reaction intermediates and products (as well as ground-state CpRh(CO)₂) are characterized with X-ray absorption spectroscopy by detecting the Rh fluorescence as a measure of Rh-specific X-ray absorption (see Supplementary Information). (**D**) Steady-state and transient Rh L_3-edge absorption spectra at indicated pump-probe time delays as well as schematic depiction of the L-edge absorption process (difference spectra are plotted relative to the edge-jump of the steady-state spectrum, intensity at 3015 eV, which is normalized to 1, steady-state and difference spectrum at delays > 190 ns are scaled for illustration). (**E, F**) Time traces (intensities versus time delay) measured at indicated X-ray photon energies with (**E**) femtosecond and (**F**) picosecond time-resolution.

the LUMO, the empty 4d-derived orbital of the Rh(I) d^8 ground state configuration. The second peak at ~3007.5 eV instead is due to transitions of Rh 2p electrons into unoccupied orbitals of mainly CO and Cp ligand character. Through metal-ligand back-donation, these ligand-derived orbitals acquire Rh 4d character and become accessible by the Rh 2p→d dipole transitions in L_3-edge XAS (*31*).

Upon laser excitation, as seen in the difference spectrum recorded at a pump-probe time delay of 250 fs, a pre-edge peak appears at ~3002.5 eV together with significant bleaching of main edge features (Fig. 1D). The temporal evolution of the pre-edge peak intensity, shown as a time trace in Fig. 1E, is well-described by a biexponential decay to a meta-stable species (see Supporting Information for kinetic model). The two time constants are assigned to CO dissociation from excited states of CpRh(CO)₂ within (370 ± 50) fs followed by octane association within (2.0 ± 0.1) ps. These assignments agree with the timescales for ligand substitution in other metal-carbonyls from previous femtosecond measurements (*26, 32*). Our experiment establishes the timescale of formation of the CpRh(CO)-octane σ-complex and the spectrum at 10 ps in Fig. 1D constitutes a direct fingerprint of how metal-ligand charge-transfer
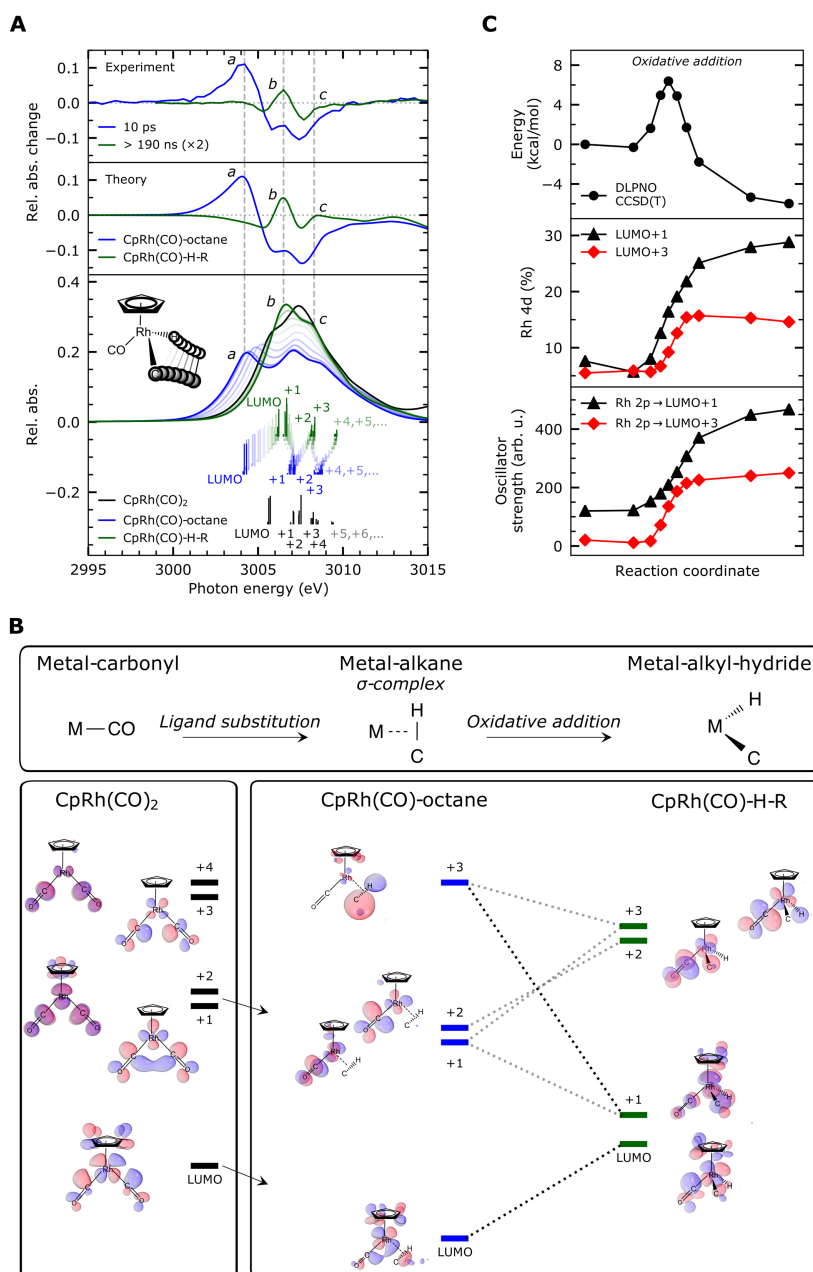
Fig. 2. X-ray absorption signatures of σ-complex formation and C-H activation by oxidative addition. (**A**) Experimental spectra at t = 10 ps and > 190 ns (top) compared to calculated spectra of CpRh(CO)-octane and CpRh(CO)-H-R (middle, calculated on the B3LYP level of theory (*40*)). L_3-edge transitions and spectra calculated for intermediate structures (bottom) illustrate the interconversion of spectral features from reactant to product along the C-H activation reaction coordinate (*37*). Calculated difference spectra are scaled such that the CpRh(CO)-octane difference spectrum matches the pre-edge intensity of the experimental spectrum at 10 ps. Vertical lines indicate positions of spectral fingerprints *a*, *b* and *c*. (**B**) Correlation diagram between the valence orbitals of CpRh(CO)₂, CpRh(CO)-octane and CpRh(CO)-H-R detailing the interconversion of orbital energies and character upon ligand substitution and C-H activation. The calculated orbital plots represent the antibonding counterpart of the bonding interactions schematically shown in Fig. 1B. For illustration, calculated orbitals are displayed with varying isovalues (see Supporting Information). (**C**) Calculated free energies (top), Rh 4d character of LUMO+1 and +3 orbitals (middle) and oscillator strengths of transitions into LUMO+1 and LUMO+3 orbitals (bottom) as a function of reaction coordinate of oxidative addition.

interactions change upon substituting a CO by an alkane ligand. On nanosecond timescales, the disappearance of the σ-complex pre-edge peak (time trace at 3004.4 eV in Fig. 1F) and the simultaneous emergence of a positive absorption feature (time trace at 3006.6 eV in Fig. 1F and transient spectrum at nanosecond delay times in Fig. 1D) reflect how the metal-ligand

charge-transfer interactions further change upon C-H activation by oxidative addition. Both time traces are modeled with a single exponential yielding a time constant of (13 ± 1) ns, in excellent agreement with the ~14 ns for C-H activation of octane with $CpRh(CO)_2$ from time-resolved IR measurements (*16*).

This assignment of the transient X-ray absorption spectra is further validated and detailed by the calculated spectra in Fig. 2A. Because shapes and intensities of the measured spectra are well-reproduced, we can robustly assign X-ray transitions to underlying charge-transfer interactions (see Supporting Information for computational details and discussion on deviations between experiment and theory). We use the experiment-theory comparison to extract the orbital correlation diagram shown in Fig. 2B. Importantly, this correlation diagram, based on robust experimental observations, relates orbital interactions from ligand substitution and σ-complex formation to C-H bond breaking and oxidative addition.

Two major effects in metal-ligand bonding of the CpRh(CO)-octane σ-complex compared to $CpRh(CO)_2$ are reflected in the 10 ps transient spectrum. First, substituting the strong-field CO ligand by the weakly-interacting octane stabilizes (decreases the energy of) the Rh 4d-derived LUMO orbital (see LUMO energy levels in Fig. 2B). This is directly reflected in a decrease of $2p \rightarrow$ LUMO transition energies: The pre-edge peak due to $2p \rightarrow$ LUMO transitions is shifted to lower energy in the σ-complex (3004.2 eV) compared to $CpRh(CO)_2$ (3006 eV, Fig. 2A). Second, an overall reduced degree of back-donation in the σ-complex compared to $CpRh(CO)_2$ lowers the hybridization of ligand orbitals with Rh 4d orbitals. This reduces intensities of the Rh 2p transitions to ligand-derived orbitals in the σ-complex and causes the depletion in the main-edge region of 3006-3009 eV (Fig. 2A).

For the subsequent C-H bond breaking and oxidative addition step from the σ-complex to the metal alkyl hydride, calculations of the free-energy landscape shown in the top panel of Fig. 2C suggest a barrier of ~7 kcal/mol and an exothermic reaction. The underlying reaction coordinate is constructed from a Nudged-Elastic-Band/TPPSh/Def2-TZVP computation (*33– 35*). Using the geometries of this reaction path scan, the free-energy landscape was computed on the DLPNO-CCSD(T)/Def2-TZVP level of theory (*36*). While we do not experimentally observe the intermediate structures along the reaction coordinate, the L_3-edge XAS spectra computed for these structures relate the spectral changes from the σ-complex reactant to the metal alkyl hydride product, which we observe. The key spectral fingerprint regions (denoted as *a*, *b* and *c* in Fig. 2A) can be assigned to excitations of Rh 2p electrons predominantly into the LUMO, LUMO+1, LUMO+2 and LUMO+3 orbitals (LUMO+4, +5, … are not discussed since they contribute to a negligible degree only). Changes of the features *a-c* hence report on the combined transformations of the four lowest unoccupied orbitals upon C-H bond breaking and oxidative addition.

In line with previous work (*37*), our calculated reaction coordinate describes the C-H bond moving towards the Rh center and, at the same time, the C-H bond elongating and breaking until the individual Rh-C and Rh-H bonds are established (cartoon in Fig 2A, bottom). These atomic rearrangements destabilize the Rh 4d-derived LUMO orbital due to increasing orbital overlap with the approaching C-H group with minor changes in hybridization (Fig. 2B and Supporting Information). The corresponding increase of $2p \rightarrow$ LUMO transition energies is directly observed experimentally by the disappearance of the pre-edge feature *a* in Fig. 2A upon transformation of the σ-complex to the alkyl hydride product: The $2p \rightarrow$ LUMO transitions shift to higher energy and merge with the main edge of the spectrum, thereby contributing to the generation of feature *b* in the spectrum of the CpRh(CO)-H-R alkyl hydride product.

LUMO+1 in the σ-complex is the energetically lowest ligand-derived orbital with dominant CO π^* character and with some Rh 4d admixture due to Rh-CO back-donation (see orbital plots

in Fig. 2B). Upon oxidative addition, LUMO+1 shifts to slightly lower energy and, importantly, gains significant Rh 4d character (see calculated Rh 4d character in Fig. 2C). The increase is so significant that the Rh 4d character becomes the dominating contribution, effectively transforming the former ligand-derived orbital into, in addition to the LUMO, a second unoccupied Rh 4d-derived orbital (see orbital plots in Fig. 2B). The increase of Rh 4d character directly scales with an increase of oscillator strength of the Rh 2p→LUMO+1 transitions (Fig. 2C). As a result, feature *b* emerges as a strong peak because it draws intensity from both, the LUMO+1 transforming into a second unoccupied Rh 4d-derived orbital and the LUMO shifting to higher energy and merging with the main edge (Fig. 2A). Feature *b* thus reflects the combined electronic-structure effects of C-H bond cleavage and oxidative addition. Oxidation of the metal center from a Rh(I) (d^8) to a Rh(III) (d^6) configuration, in particular, is evidenced by the occurrence of two unoccupied Rh 4d orbitals.

The increase of the Rh oxidation state significantly destabilizes LUMO+2 (Fig. 2B) and slightly reduces its Rh 4d character (see the calculated Rh 4d character in the Supporting information). As the second CO π^* orbital, its destabilization hence directly reflects the reduction of back-donation from the oxidized metal onto CO π^*, which has been argued to cause the shift of CO marker modes to higher energy upon C-H activation (*15*), consistent with our results. Finally, LUMO+3 in the σ-complex constitutes the octane C-H σ^* orbital with weak Rh 4d admixture due to low back-donation from Rh to C-H (orbital plot in Fig. 2B). Back-donation, however, increases as the C-H bond is broken and the covalent Rh-C and Rh-H bonds are formed and so does the Rh 4d character in LUMO+3 (Rh 4d character in Fig. 2C and orbital plots with increase in Rh 4d amplitude in Fig. 2B). Accordingly, the oscillator strengths of Rh 2p→LUMO+3 transitions strongly increase upon oxidative addition (Fig. 2C). Together with the transitions into LUMO+2 shifting towards higher energies, this explains the formation of the strong peak *c* in the alkyl hydride spectrum with an intensity similar to the steady-state spectrum of CpRh(CO)$_2$ and considerably stronger than in the σ-complex (Fig. 2A). Experimentally, this is reflected in negligible intensities in the alkyl hydride difference spectrum at the energies of feature *c* compared to the strong bleaching in the transient σ-complex spectrum.
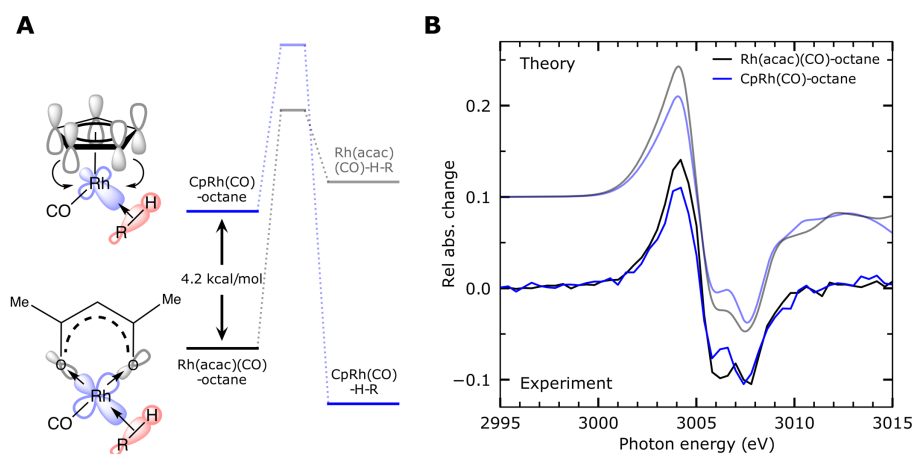
Fig. 3. X-ray orbital view on reactivity modulations in C-H activation by varying the ligand environments in σ-complexes. (**A**) Schematic of the LUMO orbitals of CpRh(CO)-octane and Rh(acac)(CO)-octane with variations in metal-ligand bonding (charge-transfer indicated by arrows) and their effect on the affinity for oxidative addition (calculated free energies). (**B**) Calculated difference spectra of CpRh(CO)-octane and Rh(acac)(CO)-octane compared to transient difference L$_3$-edge absorption spectra measured at SwissFEL at a pump-probe delay time of 10 ps. For comparison, the experimental Rh(acac)(CO)-octane spectrum is scaled to match the depletion of the CpRh(CO)-octane. This scaling is validated by the excellent agreement with the calculated spectra, which both are shown with the same scaling as in Fig. 2A (see Supporting Information).

By experimentally observing individual charge-transfer interactions including the involvement of spectator ligands, we verify and expand upon previous notions of orbital transformations along C-H activation reactions derived from quantum chemical calculations (*38*). This approach allows us to compare varying charge-transfer interactions in σ-complexes exhibiting different reactivities towards C-H activation due to different ligand environments. It has previously been shown that replacing the Cp moiety with an acetylacetonate (acac) group leads to a stable σ-complex, which, however, does not proceed to oxidative addition of the C-H bond (*39*). Our calculations shown in Fig. 3A suggest a 4.2 kcal/mol stabilization of the Rh(acac)(CO)-octane with respect to the CpRhCO-octane σ-complex. Together with the endothermic free-energy profile we calculate, this makes the C-H activated product unfavorable. We find the extra stabilization of Rh(acac)(CO)-octane to be predominantly due to a higher donation from the octane onto the Rh center. This stronger donation is favored by the higher charge deficiency at the Rh in the case of the more ionic bond between Rh and the acac group compared to Cp (see the Mulliken charges in Tab. 1).

Table 1. Mulliken charge and orbital properties of the CpRh(CO)-octane and Rh(acac)(CO)-octane σ-complexes (B3LYP level of theory).

	Rh Mulliken charge	LUMO character			
		Rh 4d (%)	Cp / acac (%)	CO (%)	Alkane (%)
CpRh(CO)-octane	0.37	39.3	28.8	4.2	6.2
Rh(acac)(CO)-octane	0.46	52.2	15.2	1.5	9.2

Our calculations predict this variation in ionicity and the related variation in reactivity for C-H activation to manifest in the XAS difference spectra of the two σ-complexes as shown in Fig. 3B. Our experiment directly confirms this prediction. In quantitative agreement with theory, the measured spectrum of Rh(acac)(CO)-octane shows a higher pre-edge intensity than CpRh(CO)-octane (Fig. 3B). We find this difference to be due to a higher Rh 4d character in the LUMO (at the expense of a lower hybridization with the acac group, see Table 1) causing the more intense 2p→LUMO pre-edge transitions in Rh(acac)(CO)-octane. This higher Rh 4d character, directly correlating with higher Rh ionicity, finally, makes the reaction step to the Rh(acac)(CO)-H-R species endothermic. A more charge-deficient Rh(I) center, in the case of acac, having a lower propensity to be further oxidized to Rh(III) is consistent with and extends established trends in alkane oxidative addition (*7*). We thus establish a direct measure of how the lower hybridization of Rh 4d with spectator-ligand orbitals in the more ionic bond to the acac ligands modulates reactivity for C-H activation by unfavorably changing the balance of charge-transfer interactions that bind (alkane-to-metal σ-donation) versus those that break the C-H bond (propensity for oxidation via metal-to-alkane back-donation).

Our results demonstrate the value of time-resolved metal-specific L-edge X-ray absorption spectroscopy for understanding, on an orbital level, what determines reactivity for C-H activation with a metal complex. We anticipate our approach to be used in the future to systematically screen σ-complexes and alkyl hydride reaction products to provide a distribution of valence orbital energies and character as measures of metal-alkane bond stability and propensity towards C-H activation with oxidative addition and, potentially, other mechanisms (*38*). We envision this to extend established trends for reactivity (*7*) by providing new experimentally verified correlations between metal-ligand charge-transfer interactions and reactivity for orbital-level control of C-H activation.

Supplementary Materials

Materials and methods, computational details, supplementary text, Figs. S1 to S10, animations of orbital transformations.

References

1. R. G. Bergman, C–H activation. *Nature*. **446**, 391–393 (2007).

2. J. A. Labinger, J. E. Bercaw, Understanding and exploiting C–H bond activation. *Nature*. **417**, 507–514 (2002).

3. B. A. Arndtsen, R. G. Bergman, T. A. Mobley, T. H. Peterson, Selective Intermolecular Carbon-Hydrogen Bond Activation by Synthetic Metal Complexes in Homogeneous Solution. *Acc. Chem. Res.* **28**, 154–162 (1995).

4. K. I. Goldberg, A. S. Goldman, Large-Scale Selective Functionalization of Alkanes. *Acc. Chem. Res.* **50**, 620–626 (2017).

5. J. K. Hoyano, A. D. McMaster, W. A. G. Graham, Activation of Methane by Iridium Complexes. *J. Am. Chem. Soc.* **105**, 7190–7191 (1983).

6. A. H. Janowicz, R. G. Bergman, Carbon-hydrogen activation in completely saturated hydrocarbons: direct observation of M + R-H .fwdarw. M(R)(H). *J. Am. Chem. Soc.* **104**, 352–354 (1982).

7. J. Hartwig, *Organotransition Metal Chemistry: From Bonding to Catalysis* (University Science Books, 2010).

8. C. Hall, R. N. Perutz, Transition Metal Alkane Complexes †. *Chem. Rev.* **96**, 3125–3146 (1996).

9. W. D. Jones, Isotope Effects in C−H Bond Activation Reactions by Transition Metals. *Acc. Chem. Res.* **36**, 140–146 (2003).

10. J. B. Asbury, H. N. Ghosh, J. S. Yeston, R. G. Bergman, T. Lian, Sub-picosecond IR study of the reactive intermediate in an alkane C-H bond activation reaction by CpRh(CO)2. *Organometallics*. **17**, 3417–3419 (1998).

11. F. M. Chadwick, T. Krämer, T. Gutmann, N. H. Rees, A. L. Thompson, A. J. Edwards, G. Buntkowsky, S. A. Macgregor, A. S. Weller, Selective C–H Activation at a Molecular Rhodium Sigma-Alkane Complex by Solid/Gas Single-Crystal to Single-Crystal H/D Exchange. *J. Am. Chem. Soc.* **138**, 13369–13378 (2016).

12. S. Geftakis, G. E. Ball, Direct Observation of a Transition Metal Alkane Complex, CpRe(CO) 2 (cyclopentane), Using NMR Spectroscopy. *J. Am. Chem. Soc.* **120**, 9953–9954 (1998).

13. J. D. Watson, L. D. Field, G. E. Ball, Binding methane to a metal centre. *Nat. Chem.* **14**, 801–804 (2022).

14. E. P. Wasserman, C. B. Moore, R. G. Bergman, Gas-Phase Rates of Alkane C-H Oxidative Addition to a Transient CpRh(CO) Complex. *Science (80-.).* **255**, 315–318 (1992).

15. S. E. Bromberg, H. Yang, M. C. Asplund, T. Lian, B. K. McNamara, K. T. Kotz, J. S. Yeston, M. Wilkens, H. Frei, R. G. Bergman, C. B. Harris, The mechanism of a C-H bond activation reaction in room-temperature alkane solution. *Science (80-.).* **278**, 260–263 (1997).

16. M. W. George, M. B. Hall, O. S. Jina, P. Portius, X.-Z. Sun, M. Towrie, H. Wu, X. Yang, S. D. Zaric, Understanding the factors affecting the activation of alkane by Cp'Rh(CO)2 (Cp' = Cp or Cp*). *Proc. Natl. Acad. Sci.* **107**, 20178–20183 (2010).

17. A. L. Pitts, A. Wriglesworth, X. Z. Sun, J. A. Calladine, S. D. Zarić, M. W. George, M. B. Hall, Carbon-hydrogen activation of cycloalkanes by cyclopentadienylcarbonylrhodium-A lifetime enigma. *J. Am. Chem. Soc.* **136**, 8614–8625 (2014).

18. M. C. Asplund, P. T. Snee, J. S. Yeston, M. J. Wilkens, C. K. Payne, H. Yang, K. T. Kotz, H. Frei, R. G. Bergman, C. B. Harris, Ultrafast UV pump/IR probe studies of C-H activation in linear, cyclic, and aryl hydrocarbons. *J. Am. Chem. Soc.* **124**, 10605–10612 (2002).

19. E. A. Cobar, R. Z. Khaliullin, R. G. Bergman, M. Head-Gordon, Theoretical study of the rhenium alkane interaction in transition metal alkane -complexes. *Proc. Natl. Acad. Sci.* **104**, 6963–6968 (2007).

20. J. Y. Saillard, R. Hoffmann, Carbon-hydrogen and hydrogen-hydrogen activation in transition metal complexes and on surfaces. *J. Am. Chem. Soc.* **106**, 2006–2026 (1984).

21. P. E. M. Siegbahn, M. Svensson, Different Electronic Structure Requirements on Precursors and Transition States for the Oxidative Addition Reaction with Methane. *J. Am. Chem. Soc.* **116**, 10124–10128 (1994).

22. D. Balcells, E. Clot, O. Eisenstein, C—H Bond Activation in Transition Metal Species from a Computational Perspective. *Chem. Rev.* **110**, 749–823 (2010).

23. R. M. Jay, K. Kunnus, P. Wernet, K. J. Gaffney, Capturing Atom-Specific Electronic Structural Dynamics of Transition-Metal Complexes with Ultrafast Soft X-Ray Spectroscopy. *Annu. Rev. Phys. Chem.* **73**, 187–208 (2022).

24. Y. Kim, R. Ma, J. Lee, J. Harich, D. Nam, S. Kim, M. Kim, M. Ochmann, I. Eom, N. Huse, J. H. Lee, T. K. Kim, Ligand-Field Effects in a Ruthenium(II) Polypyridyl Complex Probed by Femtosecond X-ray Absorption Spectroscopy. *J. Phys. Chem.*

Lett., 12165–12172 (2021).

25. B. E. Van Kuiken, N. Huse, H. Cho, M. L. Strader, M. S. Lynch, R. W. Schoenlein, M. Khalil, Probing the Electronic Structure of a Photoexcited Solar Cell Dye with Transient X-ray Absorption Spectroscopy. *J. Phys. Chem. Lett.* **3**, 1695–1700 (2012).

26. P. Wernet, K. Kunnus, I. Josefsson, I. Rajkovic, W. Quevedo, M. Beye, S. Schreck, S. Grübel, M. Scholz, D. Nordlund, W. Zhang, R. W. Hartsock, W. F. Schlotter, J. J. Turner, B. Kennedy, F. Hennies, F. M. F. De Groot, K. J. Gaffney, S. Techert, M. Odelius, A. Föhlisch, Orbital-specific mapping of the ligand exchange dynamics of Fe(CO)5 in solution. *Nature.* **520**, 78–81 (2015).

27. W. Gawelda, M. Johnson, F. M. F. De Groot, R. Abela, C. Bressler, M. Chergui, Electronic and molecular structure of photoexcited [RuII(bpy) 3]2+ probed by picosecond X-ray absorption spectroscopy. *J. Am. Chem. Soc.* **128**, 5001–5009 (2006).

28. A. A. Cordones, J. H. Lee, K. Hong, H. Cho, K. Garg, M. Boggio-Pasqua, J. J. Rack, N. Huse, R. W. Schoenlein, T. K. Kim, Transient metal-centered states mediate isomerization of a photochromic ruthenium-sulfoxide complex. *Nat. Commun.* **9**, 1989 (2018).

29. B. E. Van Kuiken, M. Valiev, S. L. Daifuku, C. Bannan, M. L. Strader, H. Cho, N. Huse, R. W. Schoenlein, N. Govind, M. Khalil, Simulating Ru L3-edge X-ray absorption spectroscopy with time-dependent density functional theory: Model complexes and electron localization in mixed-valence metal dimers. *J. Phys. Chem. A.* **117**, 4444–4454 (2013).

30. F. De Groot, Multiplet effects in X-ray spectroscopy. *Coord. Chem. Rev.* **249**, 31–63 (2005).

31. R. K. Hocking, E. C. Wasinger, F. M. F. De Groot, K. O. Hodgson, B. Hedman, E. I. Solomon, Fe L-edge XAS studies of K4[Fe(CN)6] and K 3[Fe(CN)6]: A direct probe of back-bonding. *J. Am. Chem. Soc.* **128**, 10442–10451 (2006).

32. A. G. Joly, K. A. Nelson, Metal carbonyl photochemistry in organic solvents: Femtosecond transient absorption and preliminary resonance Raman spectroscopy. *Chem. Phys.* **152**, 69–82 (1991).

33. V. Ásgeirsson, B. O. Birgisson, R. Bjornsson, U. Becker, F. Neese, C. Riplinger, H. Jónsson, Nudged Elastic Band Method for Molecular Reactions Using Energy-Weighted Springs Combined with Eigenvector Following. *J. Chem. Theory Comput.* **17**, 4929–4945 (2021).

34. J. Tao, J. P. Perdew, V. N. Staroverov, G. E. Scuseria, Climbing the Density Functional Ladder: Nonempirical Meta–Generalized Gradient Approximation Designed for Molecules and Solids. *Phys. Rev. Lett.* **91**, 146401 (2003).

35. F. Weigend, R. Ahlrichs, Balanced basis sets of split valence, triple zeta valence and quadruple zeta valence quality for H to Rn: Design and assessment of accuracy. *Phys. Chem. Chem. Phys.* **7**, 3297–3305 (2005).

36. Y. Guo, C. Riplinger, U. Becker, D. G. Liakos, Y. Minenkov, L. Cavallo, F. Neese, Communication: An improved linear scaling perturbative triples correction for the domain based local pair-natural orbital based singles and doubles coupled cluster method [DLPNO-CCSD(T)]. *J. Chem. Phys.* **148**, 011101 (2018).

37. R. H. Crabtree, E. M. Holt, M. Lavin, S. M. Morehouse, Inter- vs. intramolecular

carbon-hydrogen activation: a carbon-hydrogen-iridium bridge in [IrH2(mq)L2]BF4 and a CH + M .fwdarw. CMH reaction trajectory. *Inorg. Chem.* **24**, 1986–1992 (1985).

38.   D. H. Ess, W. A. Goddard, R. A. Periana, Electrophilic, Ambiphilic, and Nucleophilic C−H Bond Activation: Understanding the Electronic Continuum of C−H Bond Activation Through Transition-State and Reaction Pathway Interaction Energy Decompositions. *Organometallics*. **29**, 6459–6472 (2010).

39.   T. P. Dougherty, W. T. Grubbs, E. J. Heilweil, Photochemistry of Rh(CO)2(acetylacetonate) and related metal dicarbonyls studied by ultrafast infrared spectroscopy. *J. Phys. Chem.* **98**, 9396–9399 (1994).

40.   A. D. Becke, A new mixing of Hartree-Fock and local density-functional theories. *J. Chem. Phys.* **98**, 1372–1377 (1993).